

LETTER

Validation of magnetized gas-jet experiments to investigate the effects of an external magnetic field on laser-plasma instabilities

M. Bailly-Grandvaux^{1,†}, B.J. Winjum², M.J.-E. Manuel³, S. Bolaños¹,
C.A. Walsh⁴, J. Saret¹, A. Bogale¹, J. Strehlow¹, R. Lee², F. Tsung²,
W. Mori², D.H. Froula⁵, T. Filkins⁵ and F.N. Beg¹

¹Center for Energy Research, University of California San Diego, La Jolla, CA 92093, USA

²Department of Physics and Astronomy, University of California, Los Angeles, CA 95095, USA

³General Atomics, San Diego, CA 92103, USA

⁴Lawrence Livermore National Laboratory, Livermore, CA 94550, USA

⁵Laboratory For Laser Energetics, University of Rochester, Rochester, NY 14623, USA

(Received 22 March 2022; revised 6 January 2023; accepted 9 January 2023)

Laser-plasma instabilities (LPI) play a detrimental role in energy coupling to the target in inertial confinement fusion (ICF). The recent development of applied strong magnetic fields for use in ICF and laboratory astrophysics experiments has opened opportunities to investigate the role of external magnetic fields on LPIs. Recent numerical studies have shown that stimulated Raman scattering (SRS) can be mitigated by external magnetic fields in the kinetic regime of the instability and warrant systematic experimental studies to validate modelling. To this end, we design experiments at the OMEGA-EP laser facility to investigate the effect of an external perpendicular B -field of 5–30 T on the backscattered light spectrum from a gas-jet target. We present measurements from a proof-of-principle experiment, where the backward-SRS (BSRS) is in the kinetic regime, for which the magnetization is expected to produce the greatest effects on instability growth. New simulations motivated by this experiment are used to inform the proposal of an upgraded experimental design. Our simulation predictions show that the new design is suited to experimentally demonstrating BSRS mitigation by an external magnetic field, despite the magnetization effects on the hydrodynamics, as well as the inherent temporal and spatial variations in plasma conditions.

Key words: plasma instabilities, plasma dynamics

† Email address for correspondence: mbaillygrandvaux@ucsd.edu

1. Introduction

Understanding the underlying physics of laser-plasma interactions (Kruer & Dawson 1988) is extremely important for energy coupling into targets, particularly to achieve ignition in inertial confinement fusion (ICF) (Nuckolls *et al.* 1972; McCrory *et al.* 2013). Laser-plasma instabilities (LPI) such as stimulated Raman scattering (SRS), stimulated Brillouin scattering (SBS) and two-plasmon decay (TPD) can play a detrimental role in ICF. The plasma conditions (temperature, density, spatial scale and composition) and laser irradiation (spatial and temporal intensity profiles and wavelength) determine the conditions under which LPI can grow and saturate. Understanding and controlling LPI are extremely important for the success of all three main focus areas of ICF i.e. laser indirect-drive (LID) (Nuckolls *et al.* 1972), laser direct drive (LDD) (McCrory *et al.* 2013) and magnetized liner inertial fusion (MagLIF) (Slutz *et al.* 2010). For both LID and LDD, the instabilities can be strongly excited in the extended under dense plasma, for example, at the laser entrance hole (LEH) and inside the hohlraum for LID targets and coronal plasma surrounding the LDD fuel capsule. Laser beams are arranged in various cones that enter the gas-filled high-Z hohlraum from the LEH. The cross-beam energy transfer mediated by ion acoustic waves occurs at the LEH region where outer beams transfer power to inner beams when they overlap. The SRS grows continuously along the inner beam path in the long-scale-length and under-dense plasma. This can lead to a significant reduction of laser energy coupling due to the energy being scattered by SRS and SBS. In addition, SRS and TPD both involve electron plasma waves (EPWs) and can produce copious energetic hot electrons that can preheat the fusion target, degrading implosion performance.

Recent success of the MagLIF concepts (Slutz *et al.* 2010) has prompted further investigation of applying a seed magnetic field (B -field) to indirect-drive ICF implosions to enhance implosion performance (Perkins *et al.* 2013, 2017; Moody *et al.* 2020; Moody 2021; Walsh *et al.* 2022). Additionally, previous work using directly driven capsules at Omega (Chang *et al.* 2011) demonstrated that even a modest background B -field (8 T) can increase the ion temperature and neutron yield by 15 % and 30 %, respectively. A myriad of other works establishes the clear gains in ignition physics provided by a background B -field, namely thermal conduction suppression and enhanced α -particle confinement (Basko, Kemp & Meyer-ter-Vehn 2000). Magnetization of the plasma is characterized by the Hall parameter $\omega_{ce}\tau_{ei} \sim 0.3B[\text{T}] \times T_e[\text{keV}]^{3/2} \times (0.1/n_e/n_{c(3\omega)})$, where B is the magnetic field strength in units of Tesla, T_e is the electron temperature in units of kiloelectronvolts, ω_{ce} is the electron gyrofrequency, n_c is the critical density at $\lambda = 351$ nm (3ω) and τ_{ei} the electron–ion collision time. When $\omega_{ce}\tau_{ei}$ is greater than unity, the B -field can confine electrons and induce anisotropic thermal-electron diffusion. The subsequent magnetic insulation of the electron heat conduction results in hotter plasma with a prolonged lifetime, which can in turn further reduce SRS with higher T_e (increased Landau damping). Previous work by Montgomery *et al.* has demonstrated increased T_e with an externally applied parallel B -field (~ 7.5 T) in a gas-filled hohlraum; measured with 4ω optical Thomson scattering (Montgomery *et al.* 2015). Potential applications using B -fields to directly control and reduce SRS is yet to be confirmed in laser-matter experiments.

It was shown in Winjum, Tsung & Mori (2018) that a moderate strength B -field (~ 10 – 30 T) can significantly reduce the reflectivity of SRS (figure 1) in the kinetic regime of the instability. The kinetic regime corresponds to plasma conditions where the wave–particle interactions govern the SRS growth rate and where an applied magnetic field is predicted to produce the greatest changes in SRS reflectivity. This regime is attained when the dimensionless parameter $k\lambda_D$ is between ~ 0.25 and ~ 0.35 , where k

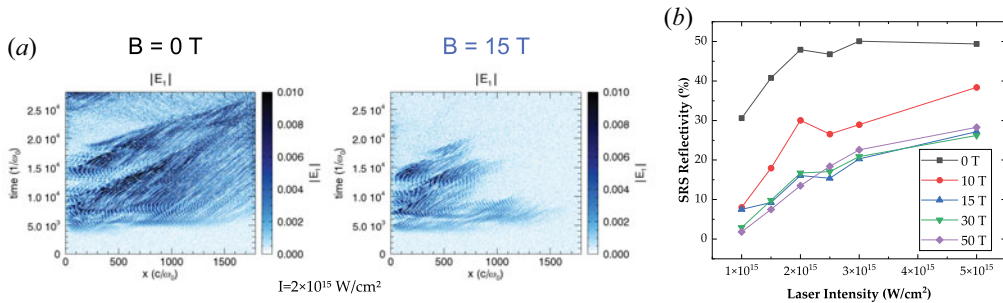


FIGURE 1. OSIRIS one-dimensional PIC simulation results. (a) Nonlinear electron plasma waves driven by SRS are shown to be heavily damped by a 15 T B -field perpendicular to the laser propagation direction at a laser intensity of $I = 2 \times 10^{15} \text{ W cm}^{-2}$ (at 3ω). (b) OSIRIS predicts suppression of SRS by moderate 10–50 T B -fields over laser intensities in the range $0.6\text{--}5 \times 10^{15} \text{ W cm}^{-2}$ (at 3ω). The simulations are all run for plasma parameters $T_e = 3 \text{ keV}$, n_e/n_c ranging from 0.128 to 0.132 within a $100 \mu\text{m}$ linear gradient, and $k\lambda_D \approx 0.30$.

is the EPW wavenumber and λ_D is the Debye length. The reduction in SRS reflectivity is most significant for a purely perpendicular B -field ($B \perp k$), due to the enhanced dissipation of nonlinear EPWs propagating perpendicular to the magnetic field. This dissipation of the EPW activity with an applied B -field perpendicular to k can be observed in the particle-in-cell (PIC) simulation results of figure 1(a). A reduction also occurs for other angles, as well as for single and multi-speckled laser beams (Winjum *et al.* 2018).

In summary, an externally applied magnetic field has been predicted to mitigate LPI by altering wave–particle interactions (Yin *et al.* 2013; Winjum *et al.* 2018) as well as to confine the plasma energy by reducing electron thermal conduction losses (Montgomery *et al.* 2015; Walsh *et al.* 2020). Magnetization of capsule implosions is an important topic for ICF due to its potential to relax the constraints of reaching ignition, as shown by the recent efforts within the national ICF program (Chang *et al.* 2011; Perkins *et al.* 2013, 2017; Moody *et al.* 2020; Moody 2021; Walsh *et al.* 2022). While SRS backscatter is not critical in present low-gas-fill LID designs, when moving to high-gain implosions, high-gas-fill targets will again be implemented wherein SRS is an important loss mechanism. Moreover, the role of preheating by SRS-driven hot electrons remains an issue, even at low gas filling. External B -field capabilities at the OMEGA laser facility are available using the MIFEDS pulsed-power device (Gotchev *et al.* 2009) and B -fields up to 30 T are readily achievable. A systematic study of the effects of an external B -field on the LPI onset and growth and their dependence on laser and plasma conditions can now be conducted at the OMEGA Laser Facility. In that context, we propose an experimental platform providing the ability to directly observe and quantify the effect of a background B -field on SRS backscatter in a well-characterized laser–plasma interaction.

2. Validation of magnetohydrodynamic simulations with data from a first experiment

We conducted a first experiment at the OMEGA-EP facility with a magnetic field of 5 T aimed at validating the feasibility of the platform and modelling capabilities. Reaching the kinetic regime for the backward-SRS (BSRS) instability requires fine control of the plasma conditions (electron temperature and density). The kinetic regime lies, for $k\lambda_D$, between ~ 0.25 and ~ 0.35 . A value of $k\lambda_D$ below or above this range results in BSRS being in the fluid regime (where no magnetic field mitigation occurs) or in the strong Landau damping

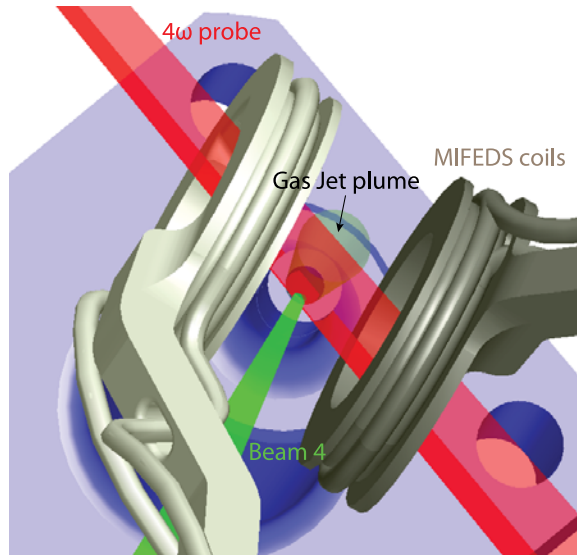


FIGURE 2. Visrad schematic of the platform as used during the first shot day. The MIFEDS coils magnetize the system. Beam 4 preheats the gas (pedestal) and then generates the scattered light spectrum, which is measured with the sub-aperture backscatter streak (SABS) diagnostic. The plasma density and temperature are characterized by the 4ω probe, X-ray spectrometer (XRS) and self-Thomson scattering (self-TS).

regime (where the BSRS reflectivity becomes marginal), respectively. We will show next that we were able to measure a BSRS spectrum in the kinetic regime with an applied B -field of 5 T.

The experimental set-up is sketched in figure 2. We used a shaped laser pulse for beam 4 comprising a foot pedestal (60 J in 300 ps, 0.2 TW, 1.3×10^{14} W cm $^{-2}$) to heat the gas prior to the interaction of the high-power part of the beam (1.25 kJ in 1 ns, 1.25 TW, 8.1×10^{14} W cm $^{-2}$). Beam 4 was equipped with a 400- μ m phase plate, giving 50 % of enclosed energy at a spot diameter of 326 μ m. Based on the measured BSRS wavelength shift (figure 5a) and temperature measurement from Ar K-shell spectroscopy, we estimated that the target peak electron density is $\sim 1.1 \times 10^{21}$ cm $^{-3}$ ($n_e/n_c \sim 13$ %) for the applied gas pressure of ~ 640 psi and the target is preheated to ~ 1 keV before the main pulse arrives at 0.45 ns. This is in agreement with pressure–density scaling laws for the gas jet (Hansen *et al.* 2018) and two-dimensional magnetohydrodynamic (MHD) simulations. We will now detail the comparison between measurements and MHD simulations.

The MHD simulations shown in figure 3 are performed in two-dimensional Cartesian geometry, using the open-source FLASH code (Dubey *et al.* 2014) with equation-of-state and multi-group opacity tables from PrOpacEOS (Golovkin & Macfarlane 2018). The magnetic field is oriented along the \hat{x} direction, that is here perpendicular to the laser propagation. The non-resistive MHD physics is activated, which specifically computes the effect of magnetic pressure via plasma advection and the anisotropy of the heat conduction due to the magnetic field, the latter using the Epperlein–Haines theory (Epperlein & Haines 1986). Concerning extended-MHD effects (Walsh *et al.* 2020), we checked with the MHD code GORGON (Walsh *et al.* 2022) that the Nernst effect was not important in this orientation. The time profiles shown in figure 3 are extracted from the simulation at each printout time step (every 50 ps), averaged in a box defined by $-100 \mu\text{m} < x < 100 \mu\text{m}$ and

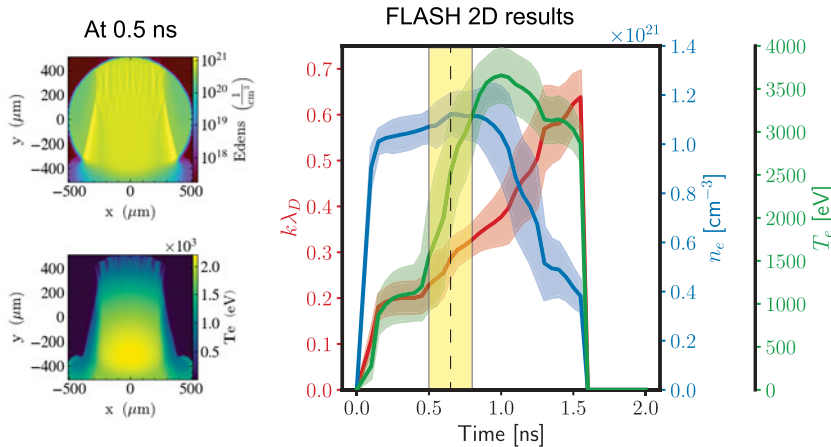


FIGURE 3. Weighted average and standard deviation of electron temperature (green curve) and density (blue curve) extracted from a FLASH-2D simulation, with the corresponding calculated $k\lambda_D$ (red curve). The yellow shaded region corresponds to the time span for which BSRS is expected to be strongly excited, matching the lifetime of the BSRS experimental signal in figure 5(a).

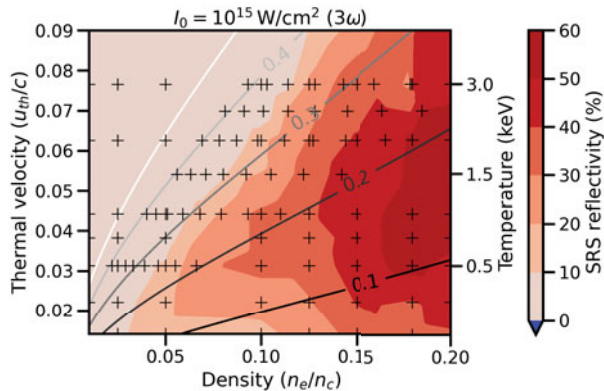


FIGURE 4. Map of backward SRS reflectivity at $B = 0$ T calculated from one-dimensional OSIRIS PIC simulations (cross symbols) across a wide range of plasma parameters. The solid lines represent contours of constant $k\lambda_D$. The map is interpolated and the resulting two-dimensional function is used to weight the average and standard deviation of plasma conditions extracted from the MHD simulations.

$-500 \mu\text{m} < y < 500 \mu\text{m}$, encompassing the laser transverse spot size and longitudinal plasma length, respectively. We calculate the average and standard deviation of plasma conditions from the MHD simulations using a weighting function that accounts for the laser energy deposition and BSRS reflectivity in each cell, in order to characterize the plasma conditions with a metric that will give prevalence to regions where the laser interacts and backscatters. The reflectivity weighting is evaluated by interpolating the results of a collection of one-dimensional electromagnetic PIC simulations using the code OSIRIS (Hemker 2000; Fonseca *et al.* 2002, 2008) performed across a wide range of plasma parameters and shown in figure 4.

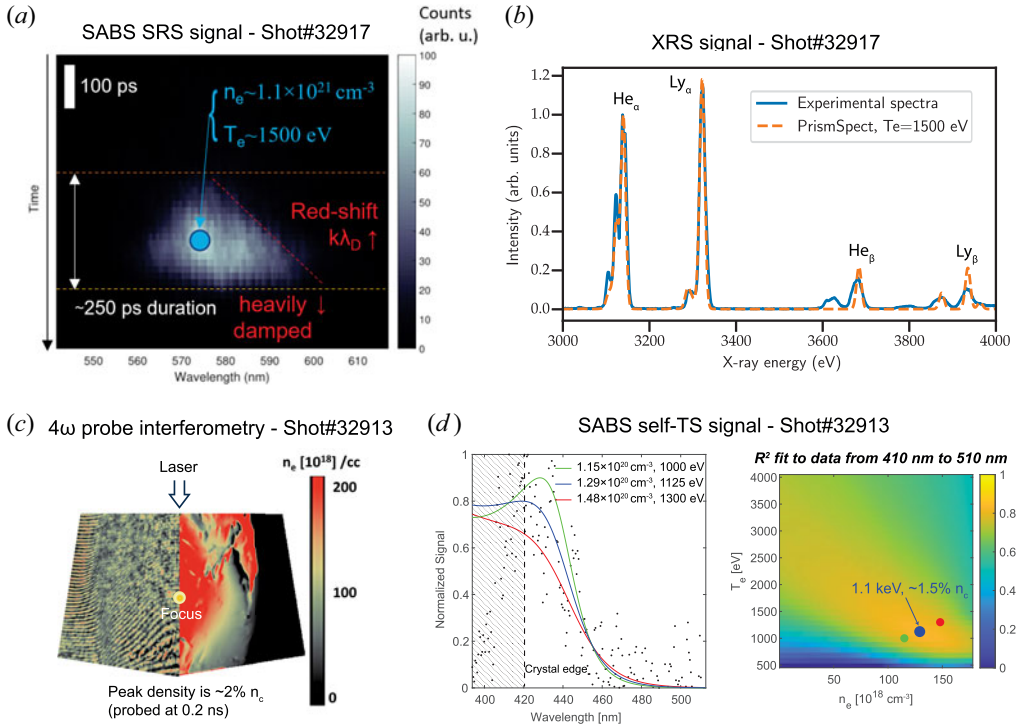


FIGURE 5. (a) The BRS signal measured by the SABS diagnostic for $B = 5$ T. The peak wavelength shift agrees well with the average conditions – at peak density – for this shot, i.e. $\sim 13\%n_c$ and ~ 1500 eV, according to FLASH (e) and XRS spectroscopy measurement (b), respectively. (b) XRS signal with a fit using the PrismSpect code, giving an electron temperature of ~ 1500 eV. For the same gas pressure, a shot with $B = 0$ T had a very different density, measured to be only $\sim 2\%n_c$ from both (c) interferometry (raw data on the left half and reconstructed density on the right half) and (d) self-TS, but showed no BRS signal due to the lower density. The three curves in the self-TS plot in (d) correspond to the best-fit conditions (R^2_{\max}) and min/max conditions at $R^2 = 0.9R^2_{\max}$. The R^2 fit map and corresponding coloured symbols for the three conditions are shown on the right side of (d).

The MHD simulation results in figure 3 show that during the interaction of the high-power main beam, the electron temperature rises quickly from ~ 1 keV to ~ 3 keV in approximately 200–300 ps. The electron temperature is ~ 2 keV when the electron density peaks, which is in reasonable agreement with the average temperature at peak density inferred from Ar K-shell spectroscopy. In figure 5(b), we show the K-shell emission collected by a time-integrated Rowland XRS (Thorn *et al.* 2018) forward fitted by synthetic spectra calculated by the collisional-radiative spectral analysis code PrismSpect (Prism Computational Sciences, Inc. 2023). Note that the fit sensitivity to opacity effects places our estimate of the average temperature in the range 1200–1600 eV. This measured average temperature is lower than inferred from MHD simulations, likely due to the underestimation of heat losses in the two-dimensional geometry. The target density then decreases due to expansion and T_e stays at its maximum.

From linear theory (Estabrook & Kruer 1983), one can relate the SRS backscattered wavelength to plasma conditions

$$\lambda_{\text{BSRS}} = 2\pi c / \sqrt{(\omega_0 - \omega_p \sqrt{1 + 3(k_{\text{EPW}} \lambda_D)^2})^2 - \omega_p^2}, \quad (2.1)$$

$$\text{where } k_{\text{EPW}} = k_L (1 + \sqrt{1 - 2\omega_p/\omega_0}), \quad (2.2)$$

where k_{EPW} is the wavenumber of the BSRS EPW. The scattered wavelength λ_{BSRS} in (2.1) depends on plasma density and temperature, respectively from the plasma frequency $\omega_p = \sqrt{n_e e^2 / m_e \epsilon_0}$ and Debye length $\lambda_D = \sqrt{\epsilon_0 k_B T_e / n_e e^2}$, with e and m_e respectively the electron charge and mass, ϵ_0 the dielectric constant, and k_B the Boltzmann constant. Here, we note that k_L is the laser wavenumber in the plasma, which writes $k_L = \sqrt{\omega_0^2 - \omega_p^2} / c$, where $\omega_0 = 2\pi c / \lambda_0$ ($\lambda_0 = 351$ nm) is the laser fundamental frequency in vacuum. This is the formalism used to calculate the $k\lambda_D$ evolution (red colour) in figure 3 from extracted MHD plasma conditions.

The simulation suggests that, during the first ~ 300 ps of the main pulse irradiation (yellow shading in figure 3), the BSRS signal would (red)-shift to larger wavelengths in time due to the increase in T_e (density is almost constant), and eventually become heavily damped ($k\lambda_D > 0.35$) approximately 150 ps after the peak density. In figure 5(a), we show the BSRS signal measured in a shot with ~ 5 T applied B -field. First, the wavelength position of the signal, accounting for the average temperature of ~ 1500 eV, yields a value of electron density in agreement with the simulation using (2.1). Moreover, we observe the redshift broadening of the BSRS signal, in line with the increasing temperature, and the signal lasts ~ 250 ps before fading, which agrees with the expected $k\lambda_D$ evolution shown in figure 3 from MHD simulations. The measurement validates the prediction from simulation and confirms the feasibility of the diagnostic for measuring BSRS in the kinetic regime of the instability ($k\lambda_D \sim 0.3$).

We also performed a shot without B -field, which resulted in a density of $n_e/n_c \sim 2\%$, according to 4ω probe interferometry (figure 5c) and self-TS from the SABS diagnostic (figure 5d). At this density, the time-averaged temperature inferred from XRS is ~ 750 eV. A FLASH simulation at $n_e/n_c \sim 2\%$ peak electron density shows electron temperatures $\sim 60\%$ lower than at $n_e/n_c \sim 13\%$, which is consistent with the XRS measurements. These plasma conditions correspond to a very large $k\lambda_D \sim 0.5$, which pertains to a strongly Landau damped regime. We can also see in figure 4 that the average reflectivity is almost zero at this very low density. Hence, as expected, no BSRS signal was observed in this shot.

Still, this low density was obtained despite firing at the same gas pressure as the shot at $n_e/n_c \sim 13\%$ (figure 5a). We suspect that the nozzle or the gas-jet valve system failed to provide the expected density on this shot. Consequently, due to this pressure-density variability and the limited number of shots at OMEGA-EP, we were not able to compare during this first experiment the BSRS signal of figure 5(a) with an unmagnetized shot at a similar density.

Moreover, the broad continuous BSRS signal observed in the magnetized shot (figure 5a) advocates for a narrower range of plasma conditions throughout the excitation beam interaction to make a clearer comparison with an unmagnetized shot. The mitigation of BSRS by the magnetic field is a kinetic effect that requires targeting of a stringent range of $k\lambda_D$ conditions. Being able to carefully characterize the MHD effects on plasma conditions is thus critical when designing an experiment that aims at demonstrating the kinetic mitigation of BSRS by an external magnetic field. We showed that FLASH MHD

simulations can successfully predict the average plasma conditions to make predictions. Besides, post-processing the MHD results using a weighting function specially designed to mimic the sensitivity of BSRS to plasma conditions allows for evaluating the effect of plasma inhomogeneity on the scattered light spectra, with and without applied B -field. Finally, note that, according to [figure 1\(b\)](#), a higher B -field strength would help increase the differences in BSRS reflectivity between the cases with and without applied B -field.

Along these lines, we detail in the next section a series of improvements to the experiments, in particular aiming at reducing the variation of plasma conditions from hydrodynamics, and carry out detailed predictions of the upgraded design using the simulation workflow presented earlier. The workflow consists of post-processing MHD simulations for the designed experiment using the aforementioned weighting function to ‘mimic’ the conditions that BSRS will be sensitive to and then run PIC simulations to calculate synthetic BSRS spectra. Our goal is to show that one can leverage the current capabilities of OMEGA-EP to design an experiment that can unambiguously demonstrate the kinetic mitigation of SRS with an external magnetic field in spite of the magnetization effects on the hydrodynamics, as well as the inherent temporal and spatial variations in plasma conditions.

3. Numerical investigation of the effects of an external B -field on plasma hydrodynamics and kinetic mitigation of BSRS in an upgraded experiment

We propose a revised platform to measure the mitigating effect of the B -field on the BSRS reflectivity in the kinetic regime. As such, this would be the first experiment to directly observe B -field effects on BSRS at ICF-relevant 3ω ($\lambda = 351$ nm) wavelengths and kinetic conditions for the SRS instability ($k\lambda_D \sim 0.3$), in line with the kinetic inflation regime of BSRS in indirect drive ICF (Kline *et al.* 2006). The collected data would also contribute to validating and constraining the modelling of BSRS under B -field influence in PIC codes such as the OSIRIS code.

The strongest mitigating effect for a specified B -field strength occurs for B perpendicular to the EPW wavenumber k . Therefore, the MIFEDS coils ideally should be aligned perpendicular to the excitation beam axis (the axis of beam 4 in [figure 2](#)). Mitigation is also more significant for stronger magnetic fields. One could generate up to ~ 30 T in the irradiated volume by orienting the MIFEDS coils along the gas-jet axis, while keeping the path of the 4ω probe beam to the target centre cleared.

[Figure 6](#) shows the parameter space for $k\lambda_D$ and for the Hall parameter $\omega_{ce}\tau_{ei}$ for values of electron density and temperature ranging from 5% n_c to 20% n_c and 500 to 3500 eV, respectively. Note that the blue ‘cloud’ symbol corresponds to the average conditions of the $B = 5$ T shot presented earlier from the first experiment, for which the value of $k\lambda_D$ for the average temperature is ~ 0.23 and the Hall parameter is $\omega_{ce}\tau_{ei} \sim 2$ with $B = 5$ T. The Hall parameter would consequently be ~ 12 for $B = 30$ T.

Given that the experimental observations described above showed that the electron temperature (and thus the value of $k\lambda_D$) evolved quickly over the ~ 250 ps BSRS emission time ([figure 3](#)), it is essential to conduct experiments that exercise sufficient control over laser and plasma fluctuations. A dedicated heater beam with a larger phase plate could be used to prepare the plasma prior to the excitation beam interaction. Its larger size would allow for improved uniformity, reducing gradients within the smaller excitation beam spot size, and its lower intensity on target would aid in avoiding filamentation during heating.

Following the heater beam, we furthermore propose a special pulse shape for the main excitation drive that would aid in the interpretation of the BSRS signal by drastically reducing temporal variations of plasma conditions during excitation. The pulse shape, selected from the available pulses of OMEGA-EP, consists of a train of up to six ~ 100

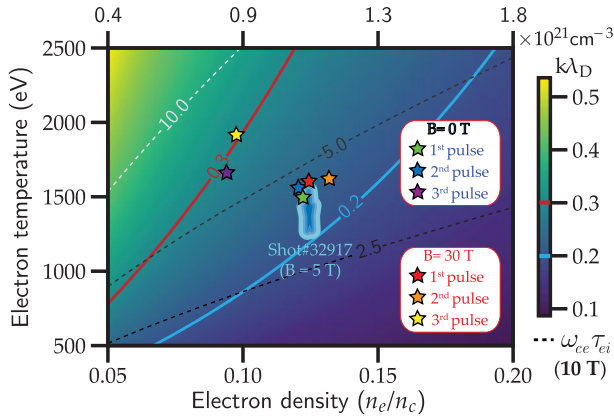


FIGURE 6. Parametric space for $k\lambda_D$ (solid line contours and colour bar) and the Hall parameter $\omega_{ce}\tau_{ei}$ (dashed line contours, for $B = 10$ T), with the electron density ranging from 5% and 20% n_c (3ω) and the electron temperature from 500 to 2500 eV. The blue ‘cloud’ symbol represents the average conditions from the magnetized shot of the first experiment. The star symbols represent the estimated conditions at each of the first three 100 ps pulses of the pulse shape proposed for the updated platform at $B = 0$ T and $B = 30$ T.

ps pulses separated by ~ 600 ps peak-to-peak (only the first three pulses should generate measurable BSRS in the present design). Note that the temporal resolution of the SABS diagnostic is ~ 80 ps Full Width at Half Maximum (FWHM), hence the evolution within the duration of 100 ps pulses would not be resolved. However, the separation between pulses would be large enough to generate discrete bursts of BSRS with a clear separation in time on the SABS diagnostic. As we observed in the magnetized shot of the first experiment (figure 5a), the continuous and rapid change of plasma temperatures makes it difficult to associate the BSRS signal with a given set of plasma conditions. In contrast, the quasi-discrete nature of the BSRS excited by short 100 ps pulses would allow for correlating the spectra to better-defined plasma conditions for each pulse that could then be compared with theory and modelling for unmagnetized and magnetized shots.

Based on these considerations, we show in figure 7 the pulse shape (a) and the conditions (n_e , T_e , $k\lambda_D$) for each of the first three 100 ps pulses for $B = 30$ T (b), as inferred from two-dimensional FLASH MHD simulations. Note that the weighting of the plasma conditions by the laser energy deposition causes the reported quantities to drop to zero when no laser is in the simulation box, i.e. between pulses. The average plasma conditions for $B = 0$ T and $B = 30$ T at the peak of each pulse extracted from FLASH using the designed BSRS weighting function are illustrated with star symbols on the density/temperature phase-space graph of figure 6, and are also reported with standard deviation in table 1.

Note that, while the average plasma conditions can change by up to $\sim 15\%$ in temperature and $\sim 9\%$ in density between unmagnetized and magnetized shots due to MHD effects, the average value of $k\lambda_D$ only changes by maximum $\sim 5\%$. The other sources of variations to consider are (i) the temporal variations within the excitation pulse duration, and (ii) the spatial variations due to inhomogeneities in plasma conditions in the interaction region. Note that temporal variations are marginal for 100 ps short pulses compared with spatial variations.

To investigate the physics of SRS under the proposed laser and plasma conditions, we used the electromagnetic PIC code OSIRIS 4.0 in one dimension. We accounted for the

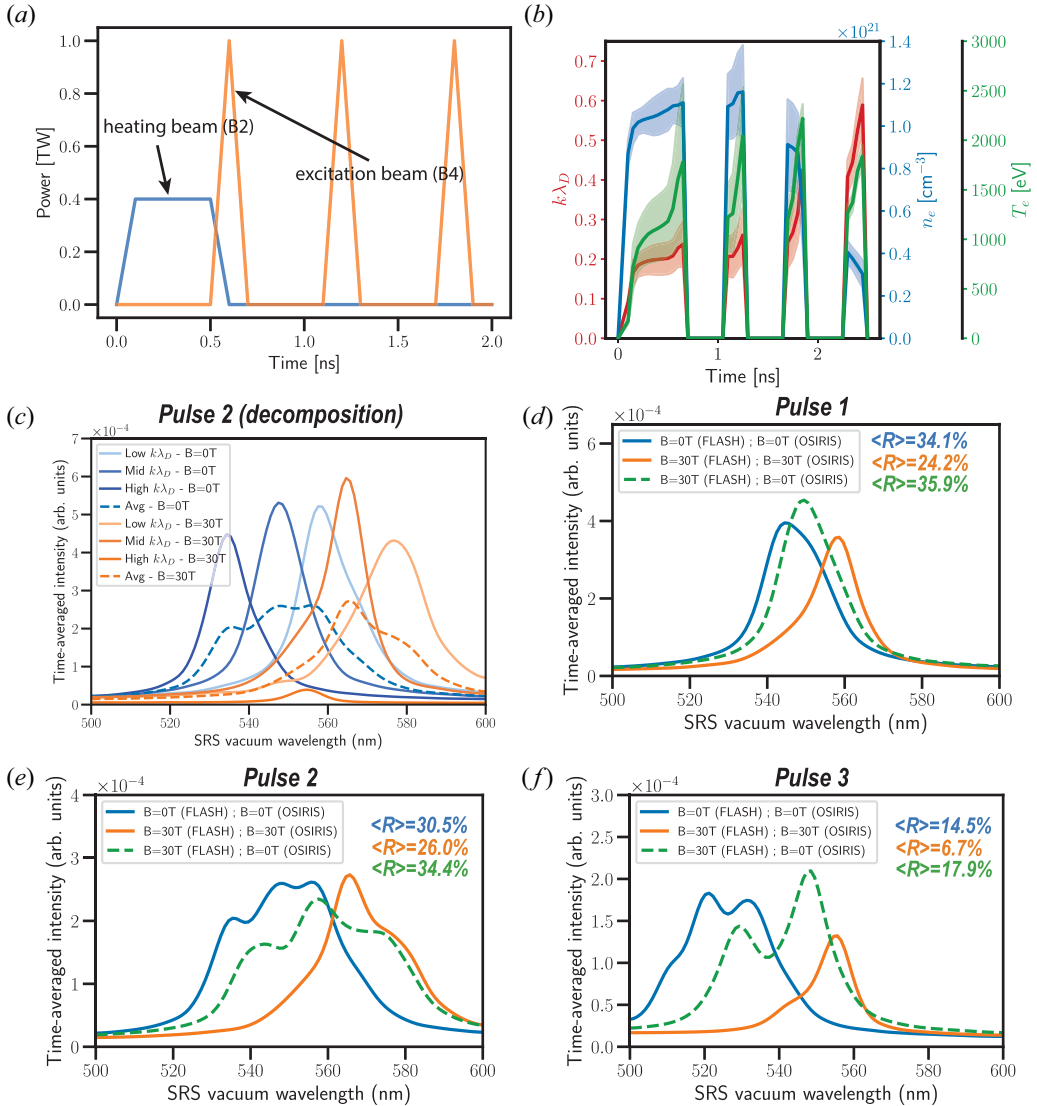


FIGURE 7. (a) Pulse shape of the proposed experiment. (b) Evolution of the electron density, $k\lambda_D$ from a two-dimensional FLASH MHD simulation with $B = 30$ T. Time-averaged light spectral density calculated by OSIRIS-1D for the conditions of the first (d), second (e) and third pulses (f), at 0 T (blue solid line) and 30 T (orange solid line). In (c), we show the decomposition of the synthetic BRS spectra of the second pulse, obtained from the mid- $k\lambda_D$ ($n_{e,avg}$, $T_{e,avg}$), the low- $k\lambda_D$ ($n_{e,avg} + \sigma_{n_e}$, $T_{e,avg} - \sigma_{T_e}$) and high- $k\lambda_D$ ($n_{e,avg} - \sigma_{n_e}$, $T_{e,avg} + \sigma_{T_e}$) conditions, where σ is the standard deviation extracted from FLASH for the respective quantity. The spectra in green dashed lines are obtained using the FLASH magnetized ($B = 30$ T) conditions, but without magnetic field in OSIRIS, thereby isolating the influence of magnetohydrodynamic on the BRS spectra excluding kinetic effects. Note that all the spectra displayed in this figure account for a spectral resolution of 5 nm FWHM. The average BRS reflectivity $\langle R \rangle$ is displayed in the plot legend for (d–f). The conditions extracted from FLASH for the first three pulses of the proposed excitation beam are shown in table 1 and the average conditions are also illustrated with star symbols of different colours in the parametric space graph of figure 6 for 0 T and 30 T.

$B(T)$	1st pulse		2nd pulse		3rd pulse	
	$n_e(\times 10^{21} \text{ cm}^{-3})$	$T_e \text{ (keV)}$	$n_e(\times 10^{21} \text{ cm}^{-3})$	$T_e \text{ (keV)}$	$n_e(\times 10^{21} \text{ cm}^{-3})$	$T_e \text{ (keV)}$
0	1.08 ± 0.08	1.46 ± 0.49	1.07 ± 0.12	1.57 ± 0.15	0.84 ± 0.11	1.67 ± 0.05
30	1.1 ± 0.09	1.61 ± 0.66	1.16 ± 0.19	1.62 ± 0.49	0.88 ± 0.19	1.92 ± 0.16

TABLE 1. Plasma conditions (average and standard deviation) extracted from the two-dimensional FLASH MHD simulation for the three pulses of the excitation beam, for $B = 0$ T and $B = 30$ T.

spatial inhomogeneities of plasma conditions in the interaction volume by considering the average and lower/upper bounds in $k\lambda_D$ obtained from the FLASH weighted quantities. All simulations were one-dimensional in Cartesian geometry. For each pulse, the plasma was initialized with the conditions extracted from MHD and weighted by the laser energy deposition and BSRS reflectivity, respectively at (i) the average electron temperature ($T_{e,\text{avg}}$) and average electron density ($n_{e,\text{avg}}$) called ‘mid- $k\lambda_D$ ’, (ii) at $T_{e,\text{avg}} + \sigma$ and $n_{e,\text{avg}} - \sigma$, called ‘high- $k\lambda_D$ ’ and (iii) at $T_{e,\text{avg}} - \sigma$ and $n_{e,\text{avg}} + \sigma$, called ‘low- $k\lambda_D$ ’, where σ is the corresponding standard deviation (see table 1). In all cases, the electron density profile had a slight linear gradient, $n_e = [0.98n_{e,\text{avg}}, 1.02n_{e,\text{avg}}]$, in order to limit the amount of forward SRS and focus on backward SRS. 1024 particles per cell with cubic interpolation, and a total of 8192 cells, were used to simulate a domain 100 μm long for a total time of 6 ps. Ions were immobile so as to focus purely on SRS. We simulate a laser beam with a wavelength of 0.351 μm and a constant intensity of $10^{15} \text{ W cm}^{-2}$, with a rise time of $300 \omega_0^{-1}$. The laser propagated in \hat{x} , was polarized in the \hat{z} direction and for simulations with an externally imposed magnetic field, $B = B_0\hat{z}$ with $B_0 = 30$ T. The boundaries were absorbing for the fields and had the plasma extending up to the boundary in all directions, with thermal bath boundaries for the particles.

In figure 7(c), we show the light spectra calculated for the low, mid and high $k\lambda_D$ conditions extracted from FLASH at the peak of the second pulse, at $B = 0$ T (shades of blues) and $B = 30$ T (shades of orange). The spectra in dashed lines are obtained by averaging the three individual spectra at the three FLASH conditions. Note that we chose to decompose the second pulse here as an example: the same methodology was applied for the two other pulses to calculate an average spectrum from the span of plasma conditions. The comparison of the $B = 0$ T and $B = 30$ T spectra shows that the B -field is mainly effective in reducing the high $k\lambda_D$ component (lower wavelengths here due to the density governing the scattered wavelength position), that is $k\lambda_D \sim 0.29$ here. On the other hand, at the low $k\lambda_D \sim 0.17$, the reflectivity is not significantly affected by the magnetic field. This is in line with the expected increasing influence of the magnetic field on BSRS as the plasma becomes more kinetic and $k\lambda_D$ approaches 0.3. The average spectra have a resulting average reflectivity of 30.5 % for $B = 0$ T and 26.0 % for $B = 30$ T.

In figure 7, we show the average backscattered light spectra for the first (d), second (e) and third (f) pulses. Note that the average reflectivity can be defined as the area under the time-average spectral intensity curves. Note also that the shifted wavelengths are within the detectable range of the SABS diagnostic, which extends from ~ 400 to ~ 800 nm, with a resolution of ~ 5 nm FWHM using a spectrometer slit width of 400 μm (value of the first experiment). The spectra from simulations are convoluted by this spectral resolution. The spectra in blue solid lines are obtained from the FLASH unmagnetized conditions and without B -field in OSIRIS. The spectra in orange solid lines are obtained

from the FLASH magnetized conditions and with $B = 30$ T in OSIRIS. To check the MHD influence on plasma conditions and the resulting BSRS light spectra, we also performed simulations using the magnetized FLASH conditions but turning off the external B -field in OSIRIS. This is equivalent to accounting for hydrodynamic effects from MHD on BSRS, yet without accounting for the kinetic effects due to the B -field in the PIC code. The results are shown by dashed green lines in (d–f). By comparing the blue $B = 0$ T and orange $B = 30$ T spectra in solid lines, it appears clearly that the BSRS reflectivities are reduced when applying the B -field. The average reflectivities are reduced by 29 %, 13 % and 54 %, for the first, second and third pulses, respectively. Moreover, based on the comparison of the orange $B = 30$ T spectra with the spectra in green dashed lines described above, it demonstrates that this reduction is caused by kinetic mitigation.

A slight increase of average BSRS reflectivity is observed for the spectra in green dashed lines compared with the blue $B = 0$ T spectra, which may look counter-intuitive given that one would expect a reduction of BSRS reflectivity in a hotter plasma. This is indeed what would occur if the density was constant between magnetized and unmagnetized cases due to the higher $k\lambda_D$ caused by the temperature increase. However, the constant density assumption is not valid. We observe instead a higher average density and a wider range of plasma conditions when magnetizing the plasma (see [table 1](#)), which leads instead to a slight increase in the average BSRS reflectivities. The reader can refer to [figure 4](#) to see the competition between a higher density and a higher temperature in terms of BSRS reflectivity and conclude that the higher density has indeed a stronger impact.

4. Conclusions

The PIC simulations have shown that a small (in terms of cyclotron frequency compared with the plasma frequency) magnetic field of a few tens of Tesla can significantly reduce the BSRS reflectivity in the kinetic regime of the instability ($k\lambda_D \sim 0.3$), due primarily to the enhanced dissipation of EPWs propagating perpendicular to a magnetic field, as well as to reduced collective SRS for multi-speckle beams. We designed a platform for the OMEGA-EP facility based on a gas-jet target, with the possibility of applying an external B -field up to 20–30 T. The first measurement of a BSRS time-resolved spectrum is presented and used to benchmark a predictive numerical workflow based on MHD and PIC simulations.

Improvements to the platform are proposed to more readily identify temporally discrete BSRS spectra for different plasma conditions. Explicitly, the use of a dedicated heater beam and a custom excitation beam pulse shape consisting of a train of short pulses is shown to strongly improve the uniformity of the plasma and yield quasi-discrete bursts of BSRS at specific times of the plasma evolution, providing the ability to quantify the effect of an external magnetic field on BSRS at various $k\lambda_D$. We validated our design with simulations showing that B -field kinetic mitigation of BSRS in the experiment would have a strong enough impact on the backscattered light spectra to be measured, in spite of spatial inhomogeneities in plasma conditions and magnetization effects on the hydrodynamics. We believe that the magnetized gas-jet design presented in this paper will be of great interest to the community for measuring magnetic field effects on various aspects of LPIs and the demonstration of BSRS B -field mitigation, in particular, will pave the way for other similar studies. Such experiments are of fundamental interest for studying laser coupling and hot electron generation in the context of ICF and exploring the uncharted behaviour of LPIs in magnetically assisted ignition schemes. Finally, to obtain a better understanding of LPIs at a fundamental level and test the validity of PIC simulations, performing experiments and collecting data are essential, especially considering the fact that LPIs experiments are quite scarce, especially under ICF-relevant laser conditions.

Acknowledgements

The experiment was conducted at the Omega Laser Facility at the University of Rochester's Laboratory for Laser Energetics with the beam time through the National Laser Users' Facility (NLUF) program.

Editor Troy Carter thanks the referees for their advice in evaluating this article.

Declaration of interest

The authors report no conflict of interest.

Funding

This material is based upon work supported by the Department of Energy, National Nuclear Security Administration under Award Numbers DE-NA0003842 and DE-NA0003856, the University of Rochester, and the New York State Energy Research and Development Authority.

Data availability statement

The data that support the findings of this study are available upon reasonable request to the corresponding author.

REFERENCES

- BASKO, M.M., KEMP, A.J. & MEYER-TER-VEHN, J. 2000 Ignition conditions for magnetized target fusion in cylindrical geometry. *Nucl. Fusion* **40** (1), 59–68.
- CHANG, P.Y., FIKSEL, G., HOHENBERGER, M., KNAUER, J.P., BETTI, R., MARSHALL, F.J., MEYERHOFER, D.D., SÉGUIN, F.H. & PETRASSO, R.D. 2011 Fusion yield enhancement in magnetized laser-driven implosions. *Phys. Rev. Lett.* **107** (3), 035006.
- DUBEY, A., ANTYPAS, K., CALDER, A.C., DALEY, C., FRYXELL, B., GALLAGHER, J.B., LAMB, D.Q., LEE, D., OLSON, K., REID, L.B., RICH, P., RICKER, P.M., RILEY, K.M., ROSNER, R., SIEGEL, A., TAYLOR, N.T., WEIDE, K., TIMMES, F.X., VLADIMIROVA, N. & ZUHONE, J. 2014 Evolution of flash, a multi-physics scientific simulation code for high-performance computing. *Intl J. High Perform. Comput. Appl.* **28** (2), 225–237.
- EPPERLEIN, E.M. & HAINES, M.G. 1986 Plasma transport coefficients in a magnetic field by direct numerical solution of the Fokker-Planck equation. *Phys. Fluids* **29** (4), 1029–1041.
- ESTABROOK, K. & KRUEER, W.L. 1983 Theory and simulation of one-dimensional Raman backward and forward scattering. *Phys. Fluids* **26** (7), 1892–1903.
- FONSECA, R.A., MARTINS, S.F., SILVA, L.O., TONGE, J.W., TSUNG, F.S. & MORI, W.B. 2008 One-to-one direct modeling of experiments and astrophysical scenarios: pushing the envelope on kinetic plasma simulations. *Plasma Phys. Control. Fusion* **50** (12), 124034. [arXiv:0810.2460](https://arxiv.org/abs/0810.2460).
- FONSECA, R.A., SILVA, L.O., TSUNG, F.S., DECYK, V.K., LU, W., REN, C., MORI, W.B., DENG, S., LEE, S., KATSIOULEAS, T. & ADAM, J.C. 2002 Osiris: a three-dimensional, fully relativistic particle in cell code for modeling plasma based accelerators. In *Computational Science — ICCS 2002* (ed. P.M.A. Sloot, A.G. Hoekstra, C.J. Kenneth Tan & J.J. Dongarra), pp. 342–351. Springer.
- GOLOVKIN, I. & MACFARLANE, J. 2018 New prism EOS and opacity tables with NLTE atomic kinetics. In *APS Division of Plasma Physics Meeting Abstracts*, APS Meeting Abstracts, vol. 2018, p. NP11.036.
- GOTCHEV, O.V., CHANG, P.Y., KNAUER, J.P., MEYERHOFER, D.D., POLOMAROV, O., FRENJE, J., LI, C.K., MANUEL, M.J.E., PETRASSO, R.D., RYGG, J.R., SÉGUIN, F.H. & BETTI, R. 2009 Laser-driven magnetic-flux compression in high-energy-density plasmas. *Phys. Rev. Lett.* **103** (21), 215004.
- HANSEN, A.M., HABERBERGER, D., KATZ, J., MASTROSIMONE, D., FOLLETT, R.K. & FROULA, D.H. 2018 Supersonic gas-jet characterization with interferometry and Thomson scattering on the OMEGA laser system. *Rev. Sci. Instrum.* **89** (10), 10C103.

- HEMKER, R.G. 2000 Particle-in-cell modeling of plasma-based accelerators in two and three dimensions. Thesis dissertation. [arXiv:1503.00276](https://arxiv.org/abs/1503.00276).
- KLINE, J.L., MONTGOMERY, D.S., YIN, L., DUBOIS, D.F., ALBRIGHT, B.J., BEZZERIDES, B., COBBLE, J.A., DODD, E.S., DUBOIS, D.F., FERNÁNDEZ, J.C., JOHNSON, R.P., KINDEL, J.M., ROSE, H.A., VU, H.X. & DAUGHTON, W. 2006 Different $k\lambda_D$ regimes for nonlinear effects on Langmuir waves. *Phys. Plasmas* **13** (5), 055906.
- KRUEER, W.L. & DAWSON, J.M. 1988 *The Physics of Laser Plasma Interactions*. Addison-Wesley Publishing Company Inc.
- MCCRORY, R.L., *et al.* 2013 Progress towards polar-drive ignition for the NIF. *Nucl. Fusion* **53** (11), 113021.
- MONTGOMERY, D.S., ALBRIGHT, B.J., BARNAK, D.H., CHANG, P.Y., DAVIES, J.R., FIKSEL, G., FROULA, D.H., KLINE, J.L., MACDONALD, M.J., SEFKOW, A.B., YIN, L. & BETTI, R. 2015 Use of external magnetic fields in hohlraum plasmas to improve laser-coupling. *Phys. Plasmas* **22** (1), 010703.
- MOODY, J.D. 2021 Boosting inertial-confinement-fusion yield with magnetized fuel. *Phys. Online J.* **14**, 51.
- MOODY, J.D., JOHNSON, A., JAVEDANI, J., CARROLL, E., FRY, J., KOZIOZIEMSKI, B., KUCHEYEV, S.O., LOGAN, B.G., POLLOCK, B.B., SIO, H., STROZZI, D., STYGAR, W.A., TANG, V. & WINTERS, S. 2020 Transient magnetic field diffusion considerations relevant to magnetically assisted indirect drive inertial confinement fusion. *Phys. Plasmas* **27** (11), 112711.
- NUCKOLLS, J., WOOD, L., THIESSEN, A. & ZIMMERMAN, G. 1972 Laser compression of matter to super-high densities: thermonuclear (CTR) applications. *Nature* **239** (5368), 139–142.
- PERKINS, L.J., HO, D.D.M., LOGAN, B.G., ZIMMERMAN, G.B., RHODES, M.A., STROZZI, D.J., BLACKFIELD, D.T. & HAWKINS, S.A. 2017 The potential of imposed magnetic fields for enhancing ignition probability and fusion energy yield in indirect-drive inertial confinement fusion. *Phys. Plasmas* **24** (6), 062708.
- PERKINS, L.J., LOGAN, B.G., ZIMMERMAN, G.B. & WERNER, C.J. 2013 Two-dimensional simulations of thermonuclear burn in ignition-scale inertial confinement fusion targets under compressed axial magnetic fields. *Phys. Plasmas* **20** (7), 072708.
- PRISM COMPUTATIONAL SCIENCES, INC. 2023Prismspect.
- SLUTZ, S.A., HERRMANN, M.C., VESEY, R.A., SEFKOW, A.B., SINARS, D.B., ROVANG, D.C., PETERSON, K.J. & CUNEO, M.E. 2010 Pulsed-power-driven cylindrical liner implosions of laser preheated fuel magnetized with an axial field^d). *Phys. Plasmas* **17** (5), 056303.
- THORN, D.B., COPPARI, F., DÖPPNER, T., MACDONALD, M.J., REGAN, S.P. & SCHNEIDER, M.B. 2018 X-ray spectrometer throughput model for (selected) flat Bragg crystal spectrometers on laser plasma facilities. *Rev. Sci. Instrum.* **89** (10), 10F119.
- WALSH, C.A., CHITTENDEN, J.P., HILL, D.W. & RIDGERS, C. 2020 Extended-magnetohydrodynamics in under-dense plasmas. *Phys. Plasmas* **27** (2), 022103.
- WALSH, C.A., FLORIDO, R., BAILLY-GRANDVAUX, M., SUZUKI-VIDAL, F., CHITTENDEN, J.P., CRILLY, A.J., GIGOSOS, M.A., MANCINI, R.C., PÉREZ-CALLEJO, G., VLACHOS, C., MCGUFFEY, C., BEG, F.N. & SANTOS, J.J. 2022 Exploring extreme magnetization phenomena in directly driven imploding cylindrical targets. *Plasma Phys. Control. Fusion* **64** (2), 025007. [arXiv:2107.13032](https://arxiv.org/abs/2107.13032).
- WALSH, C.A., O'NEILL, S., CHITTENDEN, J.P., CRILLY, A.J., APPELBE, B., STROZZI, D.J., HO, D., SIO, H., POLLOCK, B., DIVOL, L., HARTOUNI, E., ROSEN, M., LOGAN, B.G. & MOODY, J.D. 2022 Magnetized icf implosions: Scaling of temperature and yield enhancement. *Phys. Plasmas* **29** (4), 042701.
- WINJUM, B.J., TSUNG, F.S. & MORI, W.B. 2018 Mitigation of stimulated Raman scattering in the kinetic regime by external magnetic fields. *Phys. Rev. E* **98** (4), 043208. [arXiv:1802.06187](https://arxiv.org/abs/1802.06187).
- YIN, L., ALBRIGHT, B.J., ROSE, H.A., MONTGOMERY, D.S., KLINE, J.L., KIRKWOOD, R.K., MICHEL, P., BOWERS, K.J. & BERGEN, B. 2013 Self-organized coherent bursts of stimulated Raman scattering and speckle interaction in multi-speckled laser beams. *Phys. Plasmas* **20** (1), 012702.